CHARMM Fluctuating Charge Force Field for Proteins: II Protein/Solvent Properties from Molecular Dynamics Simulations Using a Nonadditive Electrostatic Model

SANDEEP PATEL, ALEXANDER D. MACKERELL, JR.,* CHARLES L. BROOKS III
Department of Molecular Biology (TPC-6), The Scripps Research Institute, 10550 N. Torrey Pines Road, La Jolla California 92037

Received 15 March 2004; Accepted 5 May 2004
DOI 10.1002/jcc.20077
Published online in Wiley InterScience (www.interscience.wiley.com).

Abstract: A fluctuating charge (FQ) force field is applied to molecular dynamics simulations for six small proteins in explicit polarizable solvent represented by the TIP4P-FQ potential. The proteins include 1FSV, 1ENH, 1PGB, 1VII, 1H8K, and 1CRN, representing both helical and β-sheet secondary structural elements. Constant pressure and temperature (NPT) molecular dynamics simulations are performed on time scales of several nanoseconds, the longest simulations yet reported using explicitly polarizable all-atom empirical potentials (for both solvent and protein) in the condensed phase. In terms of structure, the FQ force field allows deviations from native structure up to 2.5 Å (with a range of 1.0 to 2.5 Å). This is commensurate to the performance of the CHARMM22 nonpolarizable model and other currently existing polarizable models. Importantly, secondary structural elements maintain native structure in general to within 1 Å (both helix and β-strands), again in good agreement with the nonpolarizable case. In qualitative agreement with QM/MM *ab initio* dynamics on crambin (Liu et al. Proteins 2001, 44, 484), there is a sequence dependence of average condensed phase atomic charge for all proteins, a dependence one would anticipate considering the differing chemical environments around individual atoms; this is a subtle quantum mechanical feature captured in the FQ model but absent in current state-of-the-art nonpolarizable models. Furthermore, there is a mutual polarization of solvent and protein in the condensed phase. Solvent dipole moment distributions within the first and second solvation shells around the protein display a shift towards higher dipole moments (increases on the order of 0.2–0.3 Debye) relative to the bulk; protein polarization is manifested via the enhanced condensed phase charges of typical polar atoms such as backbone carbonyl oxygens, amide nitrogens, and amide hydrogens. Finally, to enlarge the sample set of proteins, gas-phase minimizations and 1 ps constant temperature simulations are performed on various-sized proteins to compare to earlier work by Kaminsky et al. (J Comp Chem 2002, 23, 1515). The present work establishes the feasibility of applying a fully polarizable force field for protein simulations and demonstrates the approach employed in extending the CHARMM force field to include these effects.

 J Comput Chem 25: 1504–1514, 2004

Key words: molecular simulations; polarizable protein force field; charge equilibration; molecular dynamics

Introduction

Classical molecular simulations are an integral tool in the theoretical study of wide-ranging physicochemical systems, including biomacromolecular systems such as proteins and DNA/RNA.[1–4] Underlying the application of classical statistical mechanical methods such as molecular dynamics and Monte Carlo is the force field, the partitioning of the quantum mechanical interactions into classical terms such as bond stretching, angle bending, dihedral rotations, out-of-plane bending, and electrostatic and dispersive interactions, which are drastically simplified as effective two-body potentials for purposes of computational efficiency.[3]

Until recently, practical force fields have included electrostatic interactions via a mean field approach where partial charges are assigned to sites defined by the force field and allowed to interact

Correspondence to: C.L. Brooks, III; e-mail: jcc.editor@scripps.edu

Contract/grant sponsor: the NIH NCRR at the Pittsburgh Supercomputing Center; contract/grant number: RR06009

Contract/grant sponsor: NIH; contract/grant number: GM51501 (to A.D.M.)

Contract/grant sponsor: The Scripps Research Institute and DOD (for computing support); contract/grant number: DAMD17-03-2-0012

via a Coulomb interaction. Electrostatic parameters (generally charges assigned to relevant sites) are determined from *ab initio* gas-phase calculations (using sophisticated approximations and levels of theory) on model compounds representing desired chemical environments; charge sets are extracted from the computed densities via fits to electrostatic potentials,[5–7] or fit to reproduce QM interaction energies and geometries of supramolecular complexes.[8,9] A final scaling procedure may be applied, in a mean-field spirit, to correct for polarization (or, in general, many-body) effects arising in the condensed phase.[5,9–11] Certainly, the application of some averaged polarization effect is deficient, particularly in interfacial regions (or more generally in cases involving strong anisotropy); this could be the liquid–vapor interface for a neat liquid or the interfacial region between protein and solvent.

The importance of accurately treating polarization in various physicochemical systems has been documented in the literature. Brooks and Foresman showed the deviation from two-body additivity of the association energy of a chloride ion with clusters of waters due to the polarization of the ion.[12] Dang et al. have implemented polarizable models for small molecules for studying liquid–vapor interfacial systems, showing evidence of surface states (free energy minima) as halides pass through the aqueous vapor–liquid interface;[13] more recently, these authors have developed a nonadditive force field for methanol, demonstrating excellent agreement of molecular dynamics simulations of the liquid at ambient conditions in reproducing liquid density, enthalpy of vaporization, liquid structure (structure factors and radial distribution functions), diffusion coefficient, and surface tension.[14] Tobias has presented similar evidence for the importance of polarization in the solvation behavior of metal ions near interfaces, specifically relating to the surface segregation of heavy halide anions in water clusters.[15]

Methods treating polarization that have found wide-spread application have been the point dipole, fluctuating charge, and Drude shell (dispersion oscillator) models.[16] The point dipole approach has found applications ranging from the study of bulk and interfacial properties of neat liquids to the calculation of free energies of ion transport across aqueous/organic interfaces.[13,17–20] The Drude model has been applied to study bulk water[21–24] and ion solvation;[25] currently, there is ongoing effort to parameterize a shell model for application to proteins and peptides.[26] The fluctuating charge method has found comparably widespread use, particularly within the last few years. Once again, it has been extensively applied to the study of various properties of bulk water, aqueous solvation of amides, hydration of the chloride ion, polyanionic systems.[27–40] Interestingly, the fluctuating charge model has been applied to implicitly solvated systems (solute treated with explicit fluctuating charges)[31] as well as coupled with QM/MM approach in which the classical region is allowed a polarization response[41] via the fluctuating charge formalism. Recently, Grossfield et al. successfully applied the AMOEBA[42] polarizable force field to compute free energies of solvation for potassium, sodium, and chloride ions in liquid water and formamide to accuracies comparable to non-polarizable models such as CHARMM27 and OPLS-AA.[43]

Unfortunately, as the above discussion suggests, the application of fully polarizable classical force fields for extended time protein dynamics simulations has not yet matured to the level of that for small molecules. There has been considerable effort over the last decade toward this goal, and advances have been made, particularly by Friesner and coworkers[44,45] Ponder et al.[43,46] and Wang et al.[47] Gresh and coworkers, with the SIBFA type point dipole potentials, have also made significant advances in the development of polarizable force fields, however, these are not yet amenable to dynamics simulations.[48–50] The majority of this work is built upon earlier studies of nonadditive models for small molecules. The work thus far has presented proof of concept; there has not been a detailed study of the effects of explicit polarization apart from the stability of a protein/peptide or DNA/RNA analog over short simulation time scales; in fact, not all cases have investigated the performance of a specific force field in the condensed phase with both explicitly polarizable solvent and solute. Furthermore, the neglect of polarization in classical simulations has been implicated many times over in situations where classical, nonpolarizable force fields fail to match or predict experimental data. Allen et al. suggest the failure of fixed-charge force fields to represent the varying dielectric environments encountered by ions passing through membrane proteins such as Gramicidin A, thus failing to reproduce ion permittivities through this model ion channel.[51] Mark and coworkers suggest the need to include explicit *solvent* polarization to accurately model relative stabilities of secondary-structural elements (helix, β-strand, extended conformation) of peptides in nonpolar (membranes) or weakly polar (methanol) media.[52] Garcia–Viloca et al. claim that substrate polarization in the dihydrofolate reductase (DHFR) catalyzed hydride transfer reaction accounts for up to 4% of the electrostatic interaction energy; they suggest that proper treatment of substrate polarization is essential for quantitative description of enzyme function and calculation of accurate binding free energies of inhibitors to proteins.[53] An interesting DFT-based study on the strengths of intrapeptide hydrogen bonding by Rossmeisl and coworkers shows polarization along the C_α—H_α bond in the direction of the carbonyl oxygen atom of the paired chain (this effect is in terms of depletion/accretion of electron density in the vicinity of the polar atoms).[54] Wang et al. described the efforts of the AMBER7 development of a nonadditive force field and its application to nanosecond-scale simulations of ubiquitin, the Dickerson dodecamer, and A- and B-DNA.[47] Liu et al. performed a 350-ps hybrid QM/MM calculation of crambin (using a self-consistent charge density functional theory (B3LYP) based tight binding scheme to model the protein and the TIP3P potential for the explicit solvent); their results indicate significant instantaneous fluctuations of atomic charges, as well as environment-dependent charge variability (i.e, backbone carbon charges vary as a function of residue).[55] This is in stark contrast to fixed-charge force fields. To date, however, there is no compelling evidence that explicit polarization is a panacea for the shortcomings of state of the art fixed-charge (mean-field) force fields and methodologies. Widespread use of explicitly polarizable force fields for studying proteins is not a reality, emphasizing the infancy of the field. But it seems that the last two statements are related; perhaps the availability of reliable polarizable force fields will eventually lead to insights not accessible with current state-of-the-art force fields thus allowing a raison d'etre for such models. In this article, we discuss the application of a previously reported fluctuating charge based force

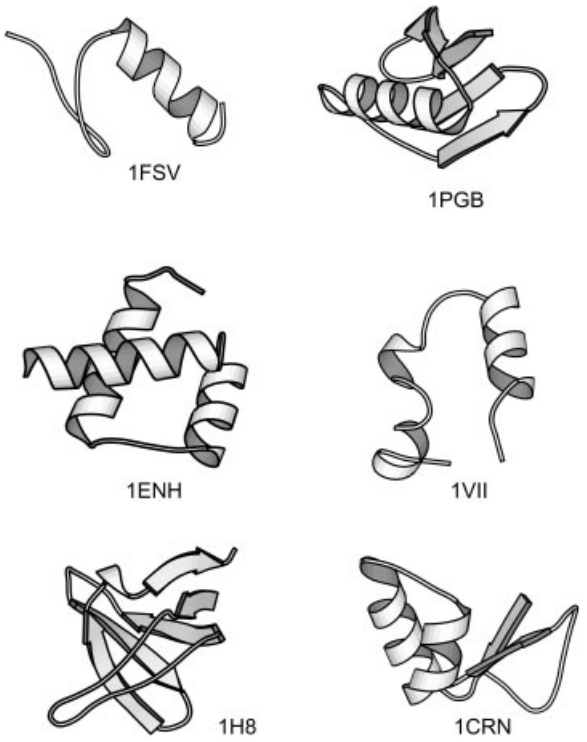

Figure 1. Test proteins explored in this study. Cartoons generated using MOLSCRIPT.[83]

field, developed in our laboratory, to simulations of explicitly solvated proteins.

In this study we consider six small proteins, shown in Figure 1, selected to include various elements of secondary structure. These include: (1) 1FSV, a 26-residue engineered protein;[56] (2) 1ENH, engrailed homeodomain; (3) 1PGB, Protein G; (4) 1VII, actin binding chicken villin headpiece; (5) 1H8K, an SH3 domain protein; and (6) 1CRN, crambin. 1FSV is a 26-residue fully designed novel protein with the α/β motif; the terminal residues (1, 2, 27, 28) are disordered and are not considered in the analysis of results (e.g., rmsd).[56] 1ENH is a 54-residue DNA-binding protein composed of three helices. 1PGB, protein G, is a 56-residue cell wall protein consisting of a four-stranded β-sheet packed against an α-helix; greater than 90% of the residues are involved in secondary structural elements.[57] These particular proteins were chosen as they are fairly small (28–57 residues) and encompass the major secondary structural units, thus allowing one to obtain sufficiently long dynamics trajectories in a reasonable amount of time. Our lab has developed a first-generation polarizable potential model, built upon the CHARMM22 all-atom scheme,[9] based on the fluctuating charge (or equivalently charge equilibration) formalism; this study will address the implementation and performance of this nonadditive potential for use in simulations of proteins in solution.

In the next section we discuss the model and methods. Then we addresses results of molecular dynamics simulations in terms of protein structure/stability, condensed phase effects specific to an explicitly polarizable force field, and vicinal solvent properties arising from polarizability. Finally, we conclude by addressing several pertinent issues.

Model and Methods

The fluctuating charge model has been applied to various systems over the last decade.[30,31,36,39,58,59] Its formalism is well documented, and the reader is directed to the relevant literature for details of the theory.[30,32,33,39,40,58,60–65] Here, we only touch upon the basics, with emphasis on issues related to application to macromolecular systems.

The total energy for a system of "M" molecules with "N" atoms each is taken as

$$E(Q, r) = \sum_{i=1}^{M} \sum_{\alpha=1}^{N_i} \chi_{i\alpha}^{o} Q_{i\alpha} + \frac{1}{2} \sum_{i=1}^{M} \sum_{j=1}^{M} \left(\sum_{\alpha=1}^{N_i} \sum_{\beta=1}^{N_j} \eta_{i\alpha j\beta} Q_{i\alpha} Q_{j\beta} + V(r_{i\alpha j\beta}) \right) \quad (1)$$

The χs are atom electronegativities (formally the Mulliken electronegativities) related to the chemical potential of an electron gas surrounding a nucleus by,[30]

$$\mu_i = \frac{\partial E}{\partial N} = -\chi_i^o = -e \frac{\partial E}{\partial q_i} \quad (2)$$

The ηs are the atom hardnesses. These values represent a "resistance" to electron flow to/from an atom. The last term in eq. (1) represents contributions from nonelectrostatic interactions, with $V(r_{i\alpha j\beta})$ including intramolecular potentials (bond stretching, angle bending, dihedral rotation, etc.) and dispersion, van der Waals interactions. The electronegativities and hardnesses are taken to be adjustable parameters; there is no *a priori* requirement that they equate to "experimental" values, a similar approach has been successfully implemented by Friesner et al. in their development efforts.[44,66,67]

Homogeneous hardness values are parameterized as discussed previously.[65] Heterogeneous elements are derived from the atom type values based on the combining rule:[61]

$$\eta_{ij}(R_{ij}, \eta_i, \eta_j) = \frac{\frac{1}{2}(\eta_i + \eta_j)}{\sqrt{1 + \frac{1}{4}(\eta_i + \eta_j)^2 R_{ij}^2}} \quad (3)$$

where R_{ij} is the separation between atoms (or more generally *sites*) i and j, and the atomic hardness parameters are the η. This local screened Coulomb potential has the correct limiting behavior as $1/R_{ij}$ for separations greater than about 2.5 Å. This interaction is computed for one to two, one to three, and one to four sites (sites included in bonds, angles, and dihedrals). Sites separated by five or more sites interact via a Coulomb interaction; in the case of interacting molecules, the interaction between sites on different molecules is again of the Coulomb form. We emphasize that this

functional form is by no means unique for the purpose at hand; it is attractive from the perspective of computational tractability and minimal computational overhead. The current parameter set, including the FQ model parameters as well as the intramolecular and nonbond potential, is available as Supplementary Material in the form of CHARMM parameter and topology files.

At this point, we address a modification of our initial parametrization protocol in light of difficulties encountered in transferring the initial parameter set from the small molecule test set to the model proteins mentioned above as well as recent evidence in the literature. Early attempts to utilize the first set of electrostatic parameters for protein simulations resulted in extreme values of charges, particularly for the polar backbone atoms such as oxygen, carbon, nitrogen, and hydrogen (essentially the elements of the peptide backbone); this suggested that the condensed-phase polarizability determined by the electrostatic parameter set may have been too high. A computational study by Morita et al. suggests that the condensed phase polarizability of water is reduced by up to 7–9% from the gas-phase value (usually cited as the molecular polarizability in the literature);[68] the implication of the study being that parameterization of polarizable models, in general, must account for this condensed-phase effect on molecular polarizability. The need, perhaps even necessity, of a reduced solution-phase polarizability has been suggested based on empirical arguments as well. There have been several reports on development of polarizable models for small, polar, hydrogen-bonding organic liquids (water, methanol) that cite the need to reduce molecular polarizability to various extents to accurately reproduce solution properties (usually vaporization enthalpies, densities, dielectric constants, diffusion constants, liquid structure, surface tension, etc.). For instance, Lamoureaux et al. reported a 28% reduction in the molecular polarizability of a Drude oscillator-based water model.[24] Recently, Dang et al. reported unphysical induction energies and forces (leading to disruption of liquid structure) using the experimental molecular polarizability in their efforts developing a nonadditive methanol model.[14] Furthermore, in ongoing work in our lab (unpublished), we have also encountered anomalous behavior in developing a methanol force field, based on the experimental molecular polarizability, in studies of liquid–vapor coexistence behavior. Thus, for the protein force field, we have scaled the hardness parameters for the backbone carbon, oxygen, nitrogen, and hydrogen atoms by a factor of 1.15 (this scaling factor allows a stable dynamics without an overpolarization in the condensed phase); we note that scaling the hardnesses effectively scales the molecular polarizability (although not linearly because not all atomic hardnesses are scaled) because the two entities are related simply, for the FQ model, as

$$\bar{\bar{\alpha}} = \Delta\bar{r}\bar{\bar{\eta}}^{-1}\Delta\bar{r}^{T} \tag{4}$$

where the $\Delta\bar{r}$ are atomic coordinates relative to the center of geometry. Following the scaling of the hardnesses, the relevant nonbonded (Lennard–Jones) parameters are refit based on condensed phase simulations. Because the backbone hardnesses are modified, the underlying backbone torsional potential is modified as discussed below. Table 1 compares the new and earlier polarizabilities for a few test molecules that contain the affected atom types; in all cases, the scaled parameters lead to polarizabilities lower than the experimental values.

Table 1. Comparison of Molecular Polarizabilities (Units of Å^3) Computed Using the Previous Unscaled[a] and Current Scaled Hardness Values.

Liquid	1/3 Tr($\bar{\bar{\alpha}}$) unscaled	1/3 Tr($\bar{\bar{\alpha}}$) scaled	Experimental
NMA	8.08	7.73	7.82
Formamide	3.23	2.7	4.01
Acetamide	5.41	4.1	5.53
Acetic acid	5.26	5.03	5.1
Imidazole	6.04	5.37	7.19

[a]Unscaled hardness values correspond to those fit in vacuum based on charge responses to dipolar probes.

With respect to charge dynamics, an extended Lagrangian formalism is used to propagate the charges in time with some general charge constraint, thus strictly providing for electronegativity equalization at each dynamics step; this in the spirit of "on-the-fly" electronic dynamics as pioneered by Car and Parinello.[69–73] Charge is normalized by residue; this effectively restricts charge flow across the peptide bond as charge is redistributed within a single residue. Further tests of allowing charge flow between residues would prove interesting. Fictitious masses are assigned to the charges; all protein charges are given the same mass on the order of 0.007 (kcal/mol)-ps^2/e,^{2} while the TIP4P-FQ waters are assigned a mass of 0.000069 (kcal/mol)-ps^2/e^2 (as reported in the original article discussing its development[30]). Despite the quadratic form of the potential, the charges can sample phase space regions not physically relevant, where the charges take on anomalous values and then diverge. This has been documented in the literature, in particular with reference to simulations of supercritical states of the TIP4P-FQ model, as well as observed in our simulations during testing and development.[27] To circumvent this, we apply a flat-bottomed, one-sided harmonic potential restraint to maintain only water charge values between specified ranges. The specification for the limits of these ranges is based on the behavior of the TIP4P-FQ models. A wall potential as suggested by Ando et al.,[27] although not applied for the current work, is implemented for use in CHARMM; the harmonic potential is preferred as it retains the quadratic form of the local electrostatic potential.

Molecular dynamics simulations were performed on solvated protein systems; the TIP4P-FQ water model represented solvent with the systems built with truncated octahedral symmetry. The simulations were performed under constant external pressure (1 atmosphere) and temperature (298 K) conditions. The nuclear degrees of freedom were coupled to a Hoover temperature bath to maintain the proper kinetic energy distribution,[74] and constant pressure was maintained via the Langevin piston method.[75] Charge degrees of freedom were also coupled to a Nose–Hoover bath with piston mass of 0.005 (kcal/mol)ps^2/e.^{2} A time step of 0.5 fs was used for numerical integration; this value for time step and charge masses leads to an acceptable level of drift from the Born–Oppenheimer (BO) surface. In the current protocol, the system is not

minimized ("quenched") to the BO surface at regular intervals (as is sometimes done with CP dynamics) during the simulation. Systems were generated by first building missing hydrogen atoms into PDB database structures of the selected proteins. Water molecules were then distributed around the solute, with overlapping molecules (closer than 5.8 Å) being deleted; we chose a rather large buffer layer from the water to prevent water molecules from penetrating too far into the van der Waal's sphere of polar atoms, which was observed to lead to an initial overpolarization of the local protein region and/or water molecule(s) and subsequent catastrophic failure of the simulation. Prior to dynamics, 200 steps of steepest descent minimization were performed; this was followed by a gradual heating to 298 K with velocity reassignment every 100 steps using a temperature increment of 30–50 K. The initial 60–80 ps are run with harmonic force constraints on backbone atoms to allow the side chains and solvent to equilibrate around the protein; the restraints are then lifted and dynamics resumed.

As mentioned above, electrostatic parameters, the atomic hardnesses and electronegativities, were determined from fits to gas-phase DFT calculations and simulations of condensed phase densities and energetics; the reader is referred to the literature for a detailed discussion of the parameterization.[65] For the moment, we discuss the backbone torsion potential. In keeping with the CHARMM development philosophy, the alanine dipeptide is considered as a model for the peptide backbone.[9,76,77] As such, the backbone torsional potential is determined by the criterion that the vacuum ϕ–ψ (adiabatic) map of the dipeptide be reproduced. For this purpose, the LMP2/cc-pVQZ//MP2/6-31G* map is taken as a benchmark. Interpolation of a difference map is used to exactly determine the backbone potential. The difference map is calculated by taking the difference between the *ab initio* map and the map (15° intervals) calculated using the original CHARMM22 torsion parameters with the fluctuating charge model; thus, any residual at the points of the map are corrected exactly, and differences between grid points are approximated via cubic spline interpolation.[78] With recent refinement, this approach allows a more accurate representation of the relative energetics (based on PDB statistics) of the various helical elements observed in known protein structures.[77] Figure 2 shows the maps for reference. Side-chain torsions are not modified; internal force constants are taken as the original CHARMM22 values. Intramolecular nonbond interactions, it has been found, must be modified as well, particularly those related to the polar backbone carbonyl oxygen and amide nitrogen; in general, this translates to an increase in the 1–4 van der Waals radius. This prevents gross deformation of the geometry around the peptide and adjacent bonds away from standard hybridization geometries of angles. Finally, energetics for ten conformers of an alanine tetrapeptide[79] are shown in Table 2, as a test of the interpolation-based potential. The energy rms error over the 10 conformers is 1.25 kcal/mol. The performance of the polarizable force fields based on OPLS/AA[66] and AMBER7 (parm99)[47] is also shown. The current force field is comparable to the original CHARMM22 force field (including a difference map correction for the backbone dihedrals) and the AMBER7 (parm99) results. It appears that the quality of the polarizable potentials correlate with the quality of the underlying additive force field, because in both the CHARMM and OPLS cases the polarizable models perform as equally well, for all intents and purposes, as the nonpolarizable models. We note that for all conformers except 1 and 3, a dihedral restraint was applied to the backbone torsion angles during minimization with the FQ force field to prevent significant deviation from the *ab initio* structure; in the absence of such restraints, the structures found the local minima on the FQ potential surface, which necessarily is different from the *ab initio* surface computed at the Hartree–Fock level (HF-6-31G*), a level of theory that neglects the dispersion interaction energy.[47]

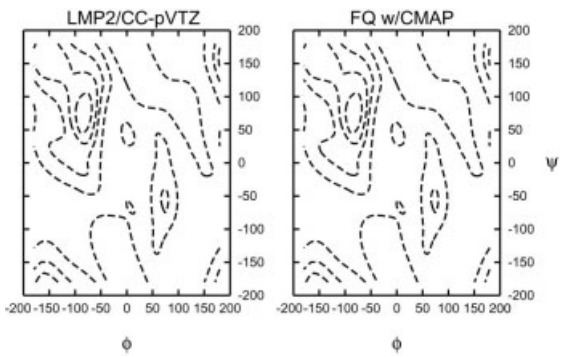

Figure 2. The alanine dipeptide adiabatic vacuum maps based on the LMP2/cc-pVQZ//MP2/6-31G* (left) and current FQ with spline interpolation (right) force fields. Contour levels are shown at 1, 2, 3, 5, and 10 kcal/mol above the global minimum.

Results and Discussion

Application to Gas-Phase Minimizations and Dynamics of Isolated Proteins

Before addressing the explicitly solvated systems, we present results of simple gas-phase simulations following the work of Kaminsky et al.[66] to have some comparison of the current parameterization with previously reported work. For a set of 22 proteins geometric rmsd values relative to the PDB structure were calculated following vacuum minimizations and short gas-phase dynamics trajectories. Table 3 shows rmsd values after vacuum conjugate gradient minimizations of each protein. The specific protocol involved initial conjugate gradient minimizations with harmonic restraints on backbone atoms to remove energetically unfavorable overlaps between side-chain atoms. Harmonic restraints were gradually lifted and unrestrained minimizations followed. One picosecond of dynamics was performed under NVT conditions with a 0.5-fs time step; the nuclear degrees of freedom were assigned initial velocities corresponding to 30 K, with heating to 298 K over 600 steps. Temperature control was maintained via velocity scaling every 0.01 ps. Table 4 lists the proteins and rmsd values after 1 ps of simulation time in the canonical ensemble; both backbone and heavy-atom values are shown. There appears to be a basin in the vicinity of 2 Å rmsd for the backbone with some exceptions. This seems to be consistent with the results of the explicitly solvated systems discussed below. The overall quality of the current FQ model based on this criterion seems

Table 2. Alanine Tetrapeptide Relative Conformer Energetics: Comparison of OPLS, AMBER, OPLS-Based Polarizable Force Field, CHARMM, and Present CHARMM-FQ Force Fields.

Conformer	*Ab initio*[a]	Charmm-FQ	CHARMM22[b]	PFF[c]	OPLS-AA/L[c]	AMBER[d] PARM99(PFF)
1	2.71	5.15	4.79	3.31	3.19	0.93
2	2.84	3.42	4.24	2.87	3.19	2.94
3	0.0	−0.70	1.00	0.14	−0.32	0.00
4	4.13	5.36	5.18	3.85	4.40	4.49
5	3.88	4.21	4.41	3.24	3.14	0.72
6	2.20	2.40	2.36	0.80	0.96	2.71
7	5.77	5.75	3.41	6.91	5.82	5.41
8	4.16	3.40	4.42	4.12	4.83	7.82
9	6.92	6.10	8.25	7.69	7.14	9.03
10	6.99	4.55	3.54	6.69	7.25	6.82
RMS error		1.25	1.67	0.69	0.56	1.70

For the CHARMM-based calculations, a uniform shift is applied to all conformer energies to minimize overall rms error from *ab initio* quantities. Energies in kcal/mol.
[a]*Ab initio* data (energies and structures) from ref. 79.
[b]CHARMM data based on difference map between ab initio map shown in Figure 2 and the CHARMM22 fixed-charge force field.
[c]Data from ref. 66.
[d]Data from ref. 47.

Table 3. Geometry rmsd (in Å) for Proteins following Gas-Phase Minimizations.

	RMSD backbone	RMSD (no hydrogens)	RMSD backbone	RMSD (no hydrogens)
PDB ID	Charmm FQ		OPLS-AA polarizable FF[a]	
1cc5	1.86	1.96	1.91	2.22
1crn	0.98	1.12	1.63	1.83
1ctf	1.18	1.84	1.65	2.18
1fdx/1dur	1.52	1.91	1.94	2.43
1paz	1.25	1.63	1.04	1.71
1pcy	1.22	1.53	1.05	1.77
1pgx	1.41	1.81	2.15	4.02
1ppt	1.58	1.79	1.70	1.90
1r69	1.21	1.60	1.13	1.70
1rnt	1.25	1.45	1.30	2.30
1sn3	0.89	1.32	1.17	2.28
1ubq	2.15	2.29	1.16	1.97
2cdv	2.37	2.76	2.37	3.53
2gn5	2.34	3.00	2.06	2.53
2lzm	1.75	2.09	1.37	1.81
2ovo	1.61	2.06	1.55	1.76
2rn2	1.36	1.93	1.09	1.54
3icb	1.7	2.13	1.47	1.82
4fd1	2.04	2.52	1.76	2.48
4pti	1.32	1.74	1.58	2.30
5cpv	1.41	1.70	1.30	1.97
7rxn	1.30	1.74	1.31	1.74
Avg.	1.53	1.91	1.53	2.17

Values are shown for the backbone and heavy-atom deviations from the Protein Data Bank structures for the current FQ parameterization and the OPLS-AA polarizable model.
[a]Data from ref. 66.

acceptable, with the average rmsd for backbone and heavy atoms being 1.53 and 1.91 Å, respectively. This is comparable to the PFF results, 1.53 and 2.17 Å, respectively, of Kaminsky et al. The average rmsd values following 1-ps molecular dynamics are 1.91 and 2.30 Å, for the current FQ model, and 1.97 and 2.66 Å for the PFF; once again, there is no systematic trend to indicate that any one potential is deficient over the span of this training set.

Protein Stability

To begin to address the quality of the FQ force field, we consider first the stability of proteins relative to the native structure over nanosecond time scales. The reference structures used for geometry rmsd calculations are as follow: 1FSV, a single average solution NMR structure (average of 41 converged structures), 1ENH, a single crystal structure (2.1 Å resolution), 1PGB, a single crystal structure (1.92 Å resolution), 1VII, a single solution NMR structure, 1H8K, a single crystal structure (2.7 Å resolution), and 1CRN, a single crystal structure of crambin (1.5 Å resolution). Figure 3 shows plots of backbone rmsd versus time for the six proteins for both the FQ and CHARMM22 nonpolarizable simulations, the latter using the TIP3P water model to which the force field is coupled; CHARMM22 calculations employing the TIP4P model (results not shown), for which the nonpolarizable force field is not rigorously parameterized, yield geometric rmsd values that are slightly poorer than with TIP3P as the solvent. The fluctuating charge force field maintains structures within 3.0 Å in keeping with the performance of the CHARMM22 nonpolarizable force field results. Any worsening of the structure may be the result of subtle interactions involved with the differing charge distributions sampled with the polarizable force field as well as a deficiency in the underlying torsion map. Furthermore, the experimental structures are of relatively low resolution, adding to the ambiguity of

Table 4. Geometry rmsd (in Å) of Protein Structures following 1-ps Gas-Phase Dynamics.

	RMSD backbone	RMSD (no hydrogens)	RMSD backbone	RMSD (no hydrogens)
PDB ID	Charmm FQ		OPLS-AA polarizable FF[a]	
1cc5	2.21	2.39	2.14	2.49
1crn	1.15	1.36	1.93	2.29
1ctf	1.90	2.39	1.75	2.33
1fdx/1dur	1.87	2.35	2.48	2.94
1paz	1.8	2.23	1.52	2.09
1pcy	1.34	1.75	1.65	2.27
1pgx	1.31	1.76	1.97	4.05
1ppt	1.84	2.32	2.32	2.82
1r69	1.60	1.98	1.40	2.27
1rnt	1.96	2.17	2.07	2.90
1sn3	1.22	1.64	1.77	2.73
1ubq	2.44	2.52	1.59	2.38
2cdv	2.64	3.14	2.12	3.5
2gn5	2.78	3.41	2.25	2.89
2lzm	2.02	2.34	1.93	2.34
2ovo	1.64	2.10	1.82	2.30
2rn2	1.62	2.10	1.7	2.17
3icb	2.03	2.43	2.19	2.5
4fd1	2.45	2.92	2.49	3.17
4pti	2.22	2.79	2.04	2.7
5cpv	1.85	2.02	1.93	2.6
7rxn	2.04	2.56	2.17	2.72
Avg.	1.91	2.30	1.97	2.66

Values for the backbone and heavy-atom deviations from Protein Data Bank structures are shown for the current FQ and OPLS-AA base polarizable models.
[a]Data from ref. 66.

the "correct" structure to compare to, particularly for 1FSV and 1VII. In fact, for 1FSV, although the overall backbone rmsd approaches 2.5 Å, the helical segment (residues 15 to 25) remains within 1.2 Å rmsd. The present results are also satisfying in that there does not appear to be a systematic deficiency in maintaining secondary structural integrity as the proteins including both helical and sheet structure show remarkably low drift from experiment. We do note that we have not studied the more subtle question of whether the FQ force field can discern between the various helical motifs (π, α, π_L). Based on recent work, we are led to believe that an accurate representation of the relative energetics of these conformations should not be expected without further manual refinement of the underlying torsional potential.[77,78] In general, however, it appears that these relatively small, flexible proteins do remain stable for significant simulation times.

Finally, we note that the current results, comparable to those observed for the nonpolarizable CHARMM22 force field, appear to be in line with those from other polarizable force fields, in particular from the AMBER and OPLS efforts. Wang et al. reported nanosecond simulations of ubiquitin and the Dickerson dodecamer (nucleic acid model); ubiquitin remained within 1.0 Å rmsd of the crystal structure.[47] Kaminsky et al. reported gas-phase NVT simulations (1 ps in length) on a set of proteins, which showed rmsd values, at the end of the simulation, ranging from 1.4 to 2.7 Å from the pdb structure.[66] Although our comparison with these latter findings is encouraging, clearly, the extremely short simulation length and lack of solvent environment must be considered as a limitation in the generality of this test.

Condensed Phase Effects

As has been observed in our, as well as others', work on bulk organic liquids, one would expect to see a polarization effect in the condensed phase. To study this, we next consider a simple probe of condensed-phase polarization, the average atomic charges in solution versus those of the vacuum minimized structure. Figure 4 shows plots of the vacuum versus average condensed phase partial atomic charge of backbone carbonyl oxygen, carbonyl carbon, amide nitrogen, and amide hydrogen atoms for each protein; averages are from the last 500–700 ps of simulation, and the vacuum charges are those associated with the gas-phase minimized structure. It is clear that there is a change in condensed phase electrostatics; furthermore, it appears that more polar atoms experience a greater charge redistribution effect. We point out that, although the polar atoms as a group show a marked polarization, there is still a spread as to the extent of polarization of individual atoms. This emphasizes the unique nature of each site, arising from the differing local chemical environments felt by each site along the protein sequence. Figure 5 shows the average charge (again from the last 500–700 ps of each simulation) on backbone atoms as a function of position along the chain. Clearly, an atom of given type experiences differing environments along the backbone. The qualitative behavior seen here is in accord with the QM/MM simulation results of Liu, Yang, and coworkers.[55] We note, however, that the current electrostatic model allows for more enhanced charges on atoms compared to QM/MM results; for instance, backbone oxygen atoms in the present study are in the range of -0.8e to -0.9e, while those in the QM/MM study range from -0.55e to -0.65e (and similarly for the carbon, nitrogen, and hydrogen atoms). This difference results, of course, from the use of different levels of theory used in the QM/MM procedure and our protocol to fit the electrostatic model parameters; in essence, the charge basis is different and in part leads to the variance in charges. Interestingly, the fluctuations in atom charges based on the FQ force field (on the order of 0.01 to 0.05 e) are commensurate to those observed with the QM/MM treatment. Figure 6 shows the average backbone atom charges and corresponding rms fluctuations versus residue for 1CRN; fluctuations for the other proteins (not shown) are similar. This suggests that the hardnesses, which in one sense represent a harmonic restraint on charges (a quadratic energy penalty for drift away from the electronegativity equalizing distribution), allow a more or less valid fluctuation of charges. Finally, apart from a sequence dependence on charge, there does not appear to be any discernible trend; for instance, one might expect common differences between sites in different secondary structural elements, or perhaps between buried and exposed residues. The lack of such behavior may be simply due to the relatively small protein sizes tested, where essentially the entire protein/peptide is "exposed" to solvent.

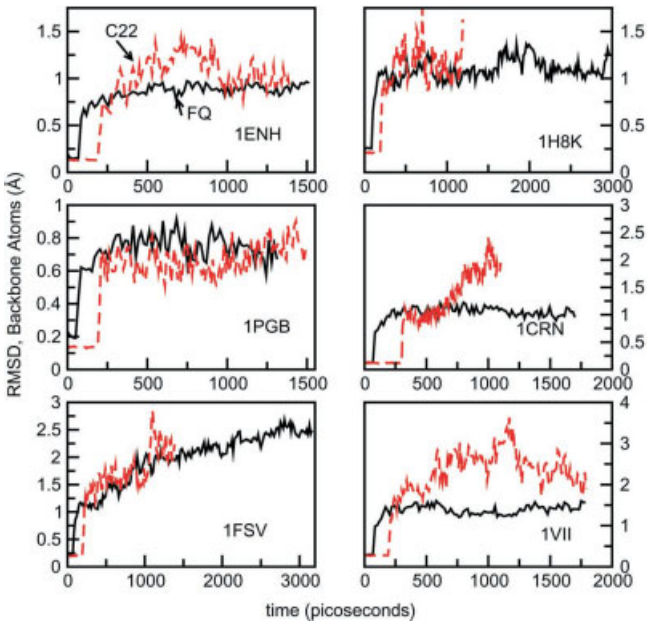

Figure 3. Backbone atom rms deviations from experimental structures for test proteins. Solid lines represent the FQ results, dashed lines the results from CHARMM22 (with TIP3P solvent) simulations.

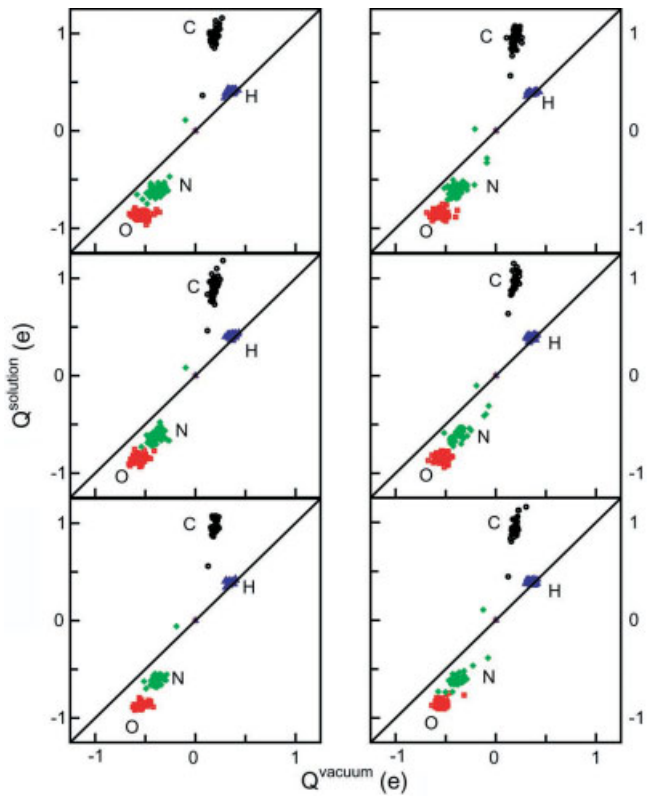

Figure 4. Vacuum versus average condensed-phase partial charge for backbone atoms. The vacuum charges are associated with the minimum gas-phase structure on the FQ potential surface.

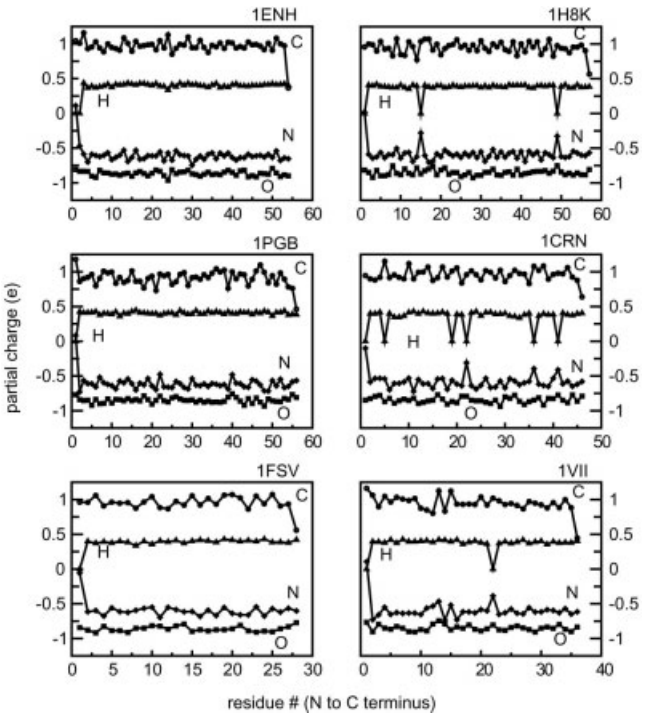

Figure 5. Average backbone atom charge vs. residue. Circles, carbonyl carbon; triangles, amide hydrogens; diamonds, amide nitrogens; squares, carbonyl oxygens. The residues where the hydrogen charge values are zero reflect the presence of a proline residue.

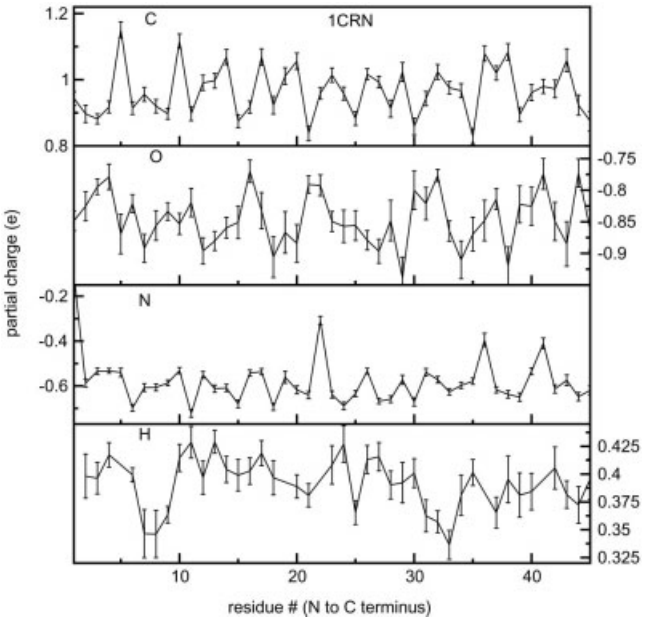

Figure 6. Average backbone atom charge and rms fluctuation vs. residue for 1CRN, crambin.

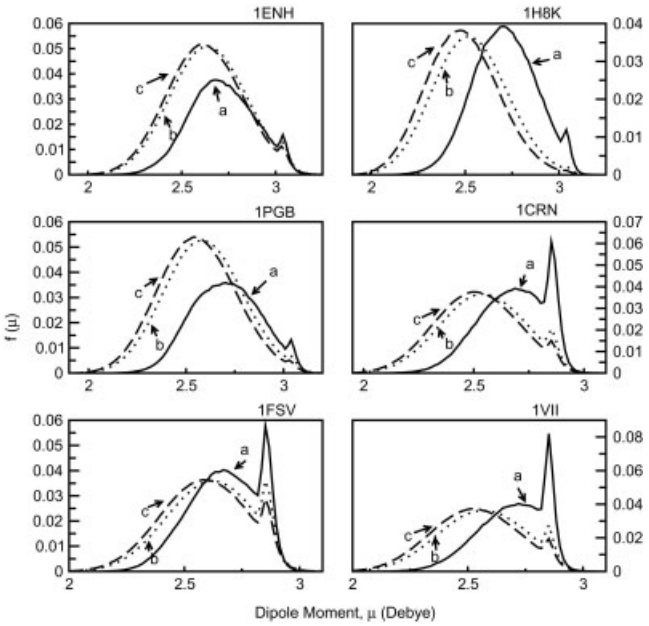

Figure 7. Water molecular dipole moment distributions as a function of water oxygen distance from backbone carbonyl oxygen atoms. Distributions calculated for water molecules in shells between: (a) 1.5 to 3.0 Å; (b) 10.0 to 12.0 Å; (c) 16.0 to 17.0 Å.

Water Properties

It is well documented in the literature that water near interfaces (i.e., vicinal water) exhibits unique properties relative to the bulk. In the present simulations, one can consider the nature of water molecules in the vicinity of the solvated peptide. Specifically, we ask about the distributions of water molecular dipole moments as one moves away from specific sites along the protein backbone. For the present analysis, we investigate the distributions with respect to both the backbone carbonyl oxygen and amide hydrogen atoms, as these sites are often involved in strong hydrogen-bonding interactions with solvent.[80] In our previous work, as well as results reported by Rick et al.[31] on amide solvation, water molecules within the first solvation shell exhibit a shift towards higher dipole moments by about 0.1 to 0.2 Debye. For the present analysis, water molecular dipole moment distributions are computed in shells, around the backbone carbonyl oxygen and amide hydrogen, from 1) 1.5 to 3.0 Å, (2) 10.0 to 12.0 Å, and (3) 16.0 to 17.0 Å (essentially bulk). Figures 7 and 8 show the distributions for each protein. The distributions for all proteins look remarkably similar, and this is not too surprising because these are averaged over all carbonyl oxygen atoms which, in terms of electrostatics (charges), are for the most part equivalent (Fig. 5). There is a systematic polarization of water molecules within the first two solvation shells (1.5 to 3.5 Å), up to on the order of 0.2 to 0.3 Debye; with concurrent polarization of the backbone oxygen atoms. This is consistent with the shift observed for TIP4P-FQ water molecules in the first solvation shell around N-methylacetamide as reported in earlier work.[31,65] One obtains the bulk-like distribution moving outward away from the proteins. It is interesting to note that there appears to be intermediate shells of water displaying distributions in between those of the bulk and first-shell, implying a gradual shift in dielectric environment (high dielectric to low dielectric) moving away from the protein–solvent interface. Although this appears to be a quite subtle behavior, it is counter to most current implementations of implicit solvation models for proteins that invariably invoke sharp dielectric boundaries. The sharp peaks at roughly 2.87 Debye result from water molecules within the first solvation shell that are directly hydrogen bonded to the carbonyl oxygen atoms; more specifically, this is a subset of molecules with carbonyl oxygen to water hydrogen distances from 1.7 to 1.8 Å (the nearest water molecules in the first solvation shell, see Fig. 9). Furthermore, this strong association with solvent occurs predominantly between carbonyl oxygen atoms associated with residues not involved in protein–protein contacts stabilizing helical and sheet structures. Finally, there is a contribution from water molecules donating to two hydrogen bonds, a scenario one would expect to give rise to strong polarization.

Conclusions

This article presents initial results of our efforts to develop and implement a fluctuating charge force field within CHARMM. Our preliminary findings, based on a sample of six small peptides/proteins, suggest the feasibility of using an explicitly polarizable force field for protein and solvent to perform meaningful dynamics simulations. This work has taken the methodology further in terms of studying several representative, fully solvated systems over nanosecond timescales rather than isolated proteins in vacuum

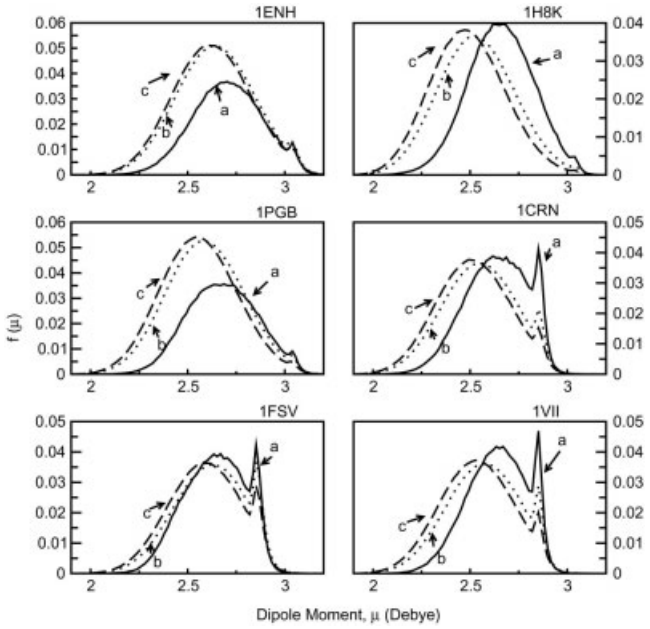

Figure 8. Water molecular dipole moment distributions as a function of water oxygen distance from backbone amide hydrogen atoms. Distributions calculated for water molecules in shells between: (a) 1.5 to 3.0 Å; (b) 10.0 to 12.0 Å; (c) 16.0 to 17.0 Å.

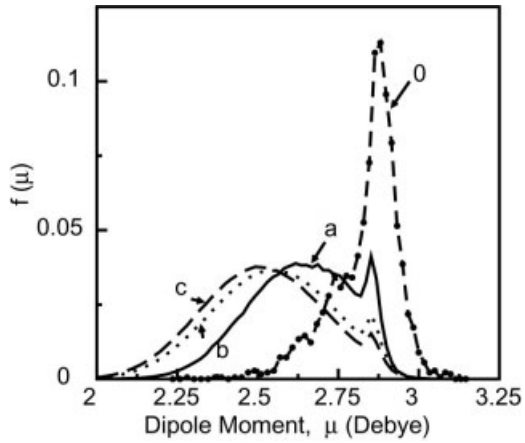

Figure 9. Water dipole movement distributions as in Figure 7. The cureve labeled "0" corresponds to water molecules within 1.8 Å of carbonyl oxygen atoms.

over picoseond time scales. In particular, the current parameterization allows for protein stability in terms of deviation from experimental native conformations; satisfyingly, secondary structural elements preserve structure to within 1 Å rmsd, equivalent to the CHARMM22 force field. Furthermore, allowing for solvent polarization provides a more realistic, physical model of proteins in solution; this cannot be achieved with current nonpolarizable models. The current parameterization also allows for the polarization of protein, as evidenced by the enhanced condensed-phase charges relative to vacuum; furthermore, for a given protein/peptide, there is a sequence-dependence of the partial atomic charge as one would expect, and is observed in low-level quantum mechanical simulations of small proteins, that is, crambin. This may be a subtle matter for gross properties, but the ability to capture charge redistribution in response to differing chemical environments, such as is the case along the protein backbone, should be important in understanding enzyme catalytic properties or chemical reactivity and/or specificity.

One should keep in mind that as with earlier reported work on the application of polarizable force fields to protein/peptide systems, the current implementation is not fully optimized, and we anticipate our CHARMM polarizable force field will continue to evolve as we explore more systems that "challenge" the current parameterization. Based on the need for a time step of 0.5 to 1.0 fs, the current approach is at least two to four times slower than a nonpolarizable CHARMM simulation using a 2.0-fs time step (fluctuating charge force field minimizations and dynamics require, respectively, 3 and 10% more CPU resources relative to the nonpolarizable force field). However, this is still competitive with point dipole models, which incur up to 20 times more CPU time for dynamics calculations than their nonpolarizable counterparts.[66] Efforts to integrate multiple-time step methods with the fluctuating charge model are anticipated to further optimize the CPU requirements of the present polarizable model.

It should be emphasized that the present polarizable force field represents a first generation that primarily combines internal parameters from the CHARMM22 nonpolarizable force field with a novel fluctuating charge electrostatic model along with optimized Lennard–Jones parameters. The initial determination of the Lennard–Jones parameters is based simply on matching liquid densities and vaporization enthalpies simultaneously with gas phase solute-water dimer geometries and energies.[65] This was done to balance solute–solute and solute–solvent interactions. However, no consideration of solvation energetics was made. One can effectively argue that accurately modeling solvation energetics of small molecules would necessarily translate to a more accurate description of the solution phase energetics of proteins. This is to be included in further development efforts. We mention that the formalism as outlined in this article may be implemented in a straightforward manner with continuum solvation models such as generalized Born.[81,82] We are currently testing such hybrid methods to reduce system size and computational overhead. Furthermore, membrane proteins such as ion channels, where polarization effects may be important for modeling of ion conductance as mentioned in the Introduction section, may be studied with implicit membrane models developed in the spirit of implicit solvation models.

References

1. Karplus, M.; McCammon, J. A. Nat Struct Bol 2002, 9, 646.
2. McCammon, J. A.; Harvey, S. C. Dynamics of Proteins and Nucleic Acids; Cambridge University Press: Cambridge, 1987.
3. Brooks, C. L., III; Karplus, M.; Pettitt, B. M. Proteins: A Theoretical Perspective of Dynamics, Structure, and Thermodynamics; John Wiley & Sons: New York, 1988.
4. Becker, O. M.; MacKerell, J., A. D.; Roux, B.; Watanabe, M., Eds. Computational Biochemistry and Biophysics; Marcel-Dekker, Inc.: New York, 2001.
5. Bayly, C. I.; Cieplak, P.; Cornell, W. D.; Kollman, P. A. J Phys Chem 1993, 97, 10269.
6. Breneman, C. M.; Wiberg, K. B. J Comp Chem 1990, 11, 361.
7. Chirlian, L. E.; Francl, M. M. J Comp Chem 1987, 8, 894.
8. Jorgensen, W. L.; Tirado–Rives, J. J Am Chem Soc 1988, 110, 1657.
9. MacKerell, A. D., Jr.; Bashford, D.; Bellott, M.; Dunbrack, R. L., Jr.; Evanseck, J. D.; Field, M. J.; Fischer, S.; Gao, J.; Guo, H.; Ha, S.; Joseph–McCarthy, D.; Kuchnir, L.; Kuczera, K.; Lau, F. T. K.; Mattos, C.; Michnick, S.; Ngo, T.; Nguyen, D. T.; Prodhom, B.; Reiher, W. E., III; Roux, B.; Schlenkrich, M.; Smith, J. C.; Stote, R.; Straub, J.; Watanabe, M.; Wiorkiewicz–Kuczera, J.; Yin, D.; Karplus, M. J Phys Chem B 1998, 102, 3586.
10. Cornell, W. D.; Cieplak, P.; Bayly, C. I.; Gould, I. R.; Merz, K. M., Jr.; Ferguson, D. M.; Spellmeyer, D. C.; Fox, T.; Caldwell, J. W.; Kollman, P. A. J Am Chem Soc 1995, 117, 5179.
11. Cornell, W. D.; Cieplak, P.; Bayly, C. I.; Kollman, P. A. J Am Chem Soc 1993, 115, 9620.
12. Foresman, J. B.; Brooks, C. L., III. J Chem Phys 1987, 87, 5892.
13. Dang, L. X. J Chem Phys 1992, 97, 2659.
14. Dang, L. X.; Chang, T.-M. J Chem Phys 2003, 119, 9851.
15. Jungwirth, P.; Tobias, D. J. J Phys Chem B 2002, 106, 6361.
16. Rick, S. W.; Stuart, S. J. Rev Comp Chem 2002, 18, 89.
17. Dang, L. X. J Phys Chem B 2001, 105, 804.
18. Caldwell, J. W.; Kollman, P. A. J Phys Chem 1995, 99, 6208.
19. Dang, L. X.; Chang, T.-M. J Chem Phys 1997, 106, 8149.
20. Chang, T.-M.; Dang, L. X.; Peterson, K. A. J Phys Chem 1997, 101, 3413.
21. Sprik, M. J Chem Phys 1991, 95, 6762.

22. Sprik, M.; Klein, M. L. J Chem Phys 1988, 89, 7556.
23. van Marren, P. J.; van der Spoel, D. J Phys Chem B 2001, 105, 2618.
24. Lamoureux, G.; Alexander D. MacKerell, J.; Roux, B. J Chem Phys 2003, 119, 5185.
25. Sprik, M.; Klein, M. L.; Watanabe, K. J Phys Chem 1990, 94, 6483.
26. Anisimov, V. M., Vorobyov, I. V., Lamoureux, G., Noskov, S., Roux, B., MacKerell, A. D., Jr. Biophys J 2004, 86, 415a.
27. Ando, K. J Chem Phys 2001, 115, 5228.
28. Krishnan, M.; Verma, A.; Balasubramanian, S. Proc Indian Acad Sci (Chem Sci) 2001, 113, 579.
29. Chen, B.; Xing, J.; Siepmann, J. I. J Phys Chem 2000, 104, 2391.
30. Rick, S. W.; Stuart, S. J.; Berne, B. J. J Chem Phys 1994, 101, 6141.
31. Rick, S. W.; Berne, B. J. J Am Chem Soc 1996, 118, 672.
32. Stuart, S. J.; Berne, B. J. J Phys Chem 1996, 100, 11934.
33. Rick, S. W.; Stuart, S. J.; Bader, J. S.; Berne, B. J. J Mol Liq 1995, 65/66, 31.
34. Ribeiro, M. C. C.; Almeida, L. C. J. J Chem Phys 1999, 110, 11445.
35. Llanta, E.; Ando, K.; Rey, R. J Phys Chem B 2001, 105, 7783.
36. Rick, S. W.; Berne, B. J. J Phys Chem B 1997, 101, 10488.
37. Yoshii, N.; Miura, S.; Okazaki, S. Chem Phys Lett 2001, 345, 195.
38. Yoshii, N.; Yoshie, H.; Miura, S.; Okazaki, S. J Chem Phys 1998, 109, 4873.
39. Rick, S. W. J Chem Phys 2001, 114, 2276.
40. Stuart, S. J.; Berne, B. J. J Phys Chem B 1999, 103, 10300.
41. Bryce, R. A.; Vincent, M. A.; Malcolm, N. O. J.; Hillier, I. H.; Burton, N. A. J Chem Phys 1998, 109, 3077.
42. Ren, P.; Ponder, J. W. J Phys Chem B 2003, 107, 5933.
43. Grossfield, A.; Ren, P.; Ponder, J. W. J Am Chem Soc 2003, 125, 15671.
44. Banks, J. L.; Kaminski, G. A.; Zhou, R.; Mainz, D. T.; Berne, B. J.; Friesner, R. A. J Chem Phys 1999, 110, 741.
45. Stern, H. A.; Rittner, F.; Berne, B. J.; Friesner, R. J Chem Phys 2001, 115, 2237.
46. Ren, P.; Ponder, J. W. J Comp Chem 2002, 23, 1497.
47. Wang, J.; Cieplak, P.; Kollman, P. A. J Comp Chem 2000, 21, 1049.
48. Gresh, N.; Garmer, D. R. J Comp Chem 1996, 17, 1481.
49. Gresh, N. J Comp Chem 1995, 16, 856.
50. Garmer, D. R.; Gresh, N.; Roques, B.-P. Proteins 1998, 31, 42.
51. Allen, T. W.; Bastug, T.; Kuyucak, S.; Chung, S.-H. Biophys J 2003, 84, 2159.
52. Soto, P.; Mark, A. E. J Phys Chem B 2002, 106, 12830.
53. Garcia–Viloca, M.; Truhlar, D. G.; Gao, J. J Mol Biol 2003, 327, 549.
54. Rossmeisl, J.; Hinnemann, B.; Jacobsen, K. W.; Norskov, J. K.; Olsen, O. H.; Pedersen, J. T. J Chem Phys 2003, 118, 9783.
55. Liu, H.; Elstner, M.; Kaxiras, E.; Frauenheim, T.; Hermans, J.; Yang, W. Proteins 2001, 44, 484.
56. Dahiyat, B. I.; Mayo, S. L. Science 1997, 278, 82.
57. Sheinerman, F. B.; Brooks, C. L., III. Proteins 1997, 29, 193.
58. Rappe, A. K.; Goddard, W. A., III. J Phys Chem 1991, 95, 3358.
59. Rick, S. W. Simulation and Theory of Electrostatic Interactions in Solution: Computational Chemistry, Biophysics, and Aqueous Solutions, Pratt, L. R. and Hummer G., eds. American Institute of Physics. Santa Fe, NM, 1999.
60. Parr, R. G.; Yang, W. Density-Functional Theory of Atoms and Molecules; Oxford University Press: Oxford, 1989.
61. Nalewajski, R. F.; Korchowiec, J.; Zhou, Z. Int J Quantum Chem: Quantim Chem Symp 1988, 22, 349.
62. Sanderson, R. T. Science 1951, 114, 670.
63. Sanderson, R. T. Chemical Bonds and Bond Energy; Academic: New York, 1976.
64. York, D. M.; Yang, W. J Chem Phys 1996, 104, 159.
65. Patel, S.; Brooks, C. L., III. J Comp Chem 2004, 25, 1.
66. Kaminski, G. A.; Stern, H. A.; Berne, B. J.; Friesner, R. A.; Cao, Y. X.; Murphy, R. B.; Zhou, R.; Halgren, T. A. J Comp Chem 2002, 23, 1515.
67. Stern, H. A.; Kaminski, G. A.; Banks, J. L.; Zhou, R.; Berne, B. J.; Friesner, R. A. J Phys Chem B 1999, 103, 4730.
68. Morita, A. J Comp Chem 2002, 23, 1466.
69. Nose, S. Mol Phys 1984, 52, 255.
70. Andersen, H. C. J Chem Phys 1980, 72, 2384.
71. Parrinello, M.; Rahman, A. Phys Rev Lett 1980, 45, 1196.
72. Car, R.; Parrinello, M. Phys Rev Lett 1985, 55, 2471.
73. Pastore, G.; Smargiassi, E.; Buda, F. Phys Rev A 1991, 44, 6334.
74. Martyna, G. J.; Klein, M. L.; Tuckerman, M. J Chem Phys 1992, 97, 2635.
75. Allen, M. P.; Tildesley, D. J. Computer Simulation of Liquids; Clarendon Press: Oxford, 1987.
76. MacKerell , A. D., Jr.; Feig, M.; Brooks, C. L., III. J Am Chem Soc 2004, 126, 698.
77. MacKerell , A. D., Jr.; Feig, M.; Brooks, C. L., III. J Comp Chem 2004, 25, 1400.
78. Feig, M.; MacKerell , A. D., Jr.; Brooks, C. L., III. J Phys Chem B 2003, 107, 2831.
79. Beachy, M. D.; Chasman, D.; Murphy, R. B.; Halgren, T. A.; Friesner, R. A. J Am Chem Soc 1997, 119, 5908.
80. Baker, E. N.; Hubbard, R. E. Prog Biophys Molec Biol 1984, 44, 97.
81. Im, W.; Lee, M. S.; Brooks, C. L., III. J Comp Chem 2003, 24, 1691.
82. Lee, M. S.; Salsbury, F. R., Jr.; Brooks, C. L., III. J Chem Phys 2002, 116, 10606.
83. Kraulis, P. J. J Appl Crystallogr 1991, 24, 946.